O. Kepka* and C. Royon†
DAPNIA/Service de physique des particules, CEA/Saclay, 91191 Gif-sur-Yvette cedex, France

C. Marquet‡
RIKEN BNL Research Center, Brookhaven National Laboratory, Upton, NY 11973, USA

R. Peschanski§
Service de physique théorique, CEA/Saclay, 91191 Gif-sur-Yvette cedex, France
URA 2306, unité de recherche associée au CNRS

We show that the forward-jet measurements performed at HERA allow for a detailed study of corrections due to next-leading logarithms (NLL) in the Balitsky-Fadin-Kuraev-Lipatov (BFKL) approach. While the description of the $d\sigma/dx$ data shows small sensitivity to NLL-BFKL corrections, these can be tested by the triple differential cross-section $d\sigma/dxdk_T^2dQ^2$ recently measured. These data can be successfully described using a renormalisation-group improved NLL kernel while the standard next-leading-order QCD or leading-logarithm BFKL approaches fail to describe the same data in the whole kinematic range. We present a detailed analysis of the NLL-scheme and renormalisation-scale dependences and also discuss the photon impact factors.

I. INTRODUCTION

Forward-jet production in lepton-proton deep inelastic scattering is a process in which a jet is detected at forward rapiditites in the direction of the proton. This process is characterized by two hard scales: Q^2, the virtuality of the intermediate photon that undergoes the hadronic interaction and k_T^2, the squared transverse momentum of the forward jet. When the total energy of the photon-proton collision W is sufficiently large, corresponding to a small value of the Bjorken variable $x \simeq Q^2/W^2$, forward-jet production is relevant [1] for testing the Balitsky-Fadin-Kuraev-Lipatov (BFKL) approach [2].

In fixed-order perturbative QCD calculations, the hard cross section is computed at fixed order with respect to α_s, and large logarithms coming from the strong ordering between the proton scale and the forward-jet scale are resummed using the Dokshitzer-Gribov-Lipatov-Altarelli-Parisi (DGLAP) evolution equation [3]. However in the small$-x$ regime, other large logarithms arise in the hard cross section itself, due to the strong ordering between the energy W and the hard scales. These can be resummed using the BFKL equation, at leading (LL) and next-leading (NLL) logarithmic accuracy [2, 4].

It has been shown that the H1 and ZEUS $d\sigma/dx$ forward-jet data [5, 6, 7] are well described by LL-BFKL predictions [8, 10], while fixed-order perturbative QCD predictions at next-to-leading order (NLOQCD) fail to describe the data, underestimating the cross-section by a factor of about 2 at small values of x. However, these tests on the relevance of BFKL dynamics have not been considered fully conclusive. On the theoretical side, it has been found that NLL-BFKL corrections [4] could be large enough to invalidate the tests. On a phenomenological side, other models such as DGLAP evolution with a "resolved" photon [9] could increase the NLOQCD predictions and come to a resonable agreement with the data.

Recent experimental forward-jet results [5, 6] motivate a new phenomenological analysis of BFKL effects in forward-jet cross-sections. In particular the triple-differential cross-section $d\sigma/dxdk_T^2dQ^2$, allows for a detailed study of the QCD dynamics of forward jets. Contrary to the $d\sigma/dx$ data, which were obtained with kinematical cuts such that $r = k_T^2/Q^2 \sim 1$, the triple differential cross-section is measured with different sets of cuts such that the data are also sensitive to the region $r \gg 1$. While LL-BFKL predictions describe well the data obtained with $r \sim 1$, it was noticed [10] that they fail to describe the $r \gg 1$ regime, indicating the need for NLL-BFKL corrections.

It was known that NLL-BFKL corrections could be large due to the appearance of spurious singularities in contradiction with renormalization-group requirements. However it has been realised [11, 12] that a renormalisation-group

*Electronic address: oldrich.kepka@cea.fr
†Electronic address: royon@hep.saclay.cea.fr
‡Electronic address: marquet@quark.phy.bnl.gov
§Electronic address: pesch@spht.saclay.cea.fr

improved NLL-BFKL regularisation can solve the singularity problem and lead to reasonable NLL-BFKL kernels (see also [13] for different approaches). This motivates the present phenomenological study of NLL-BFKL effects in forward-jet production. Even though the determination of the next-leading impact factors is still in progress [14], our analysis allows to study the NNL-BFKL framework, and the remaining ambiguity corresponding to the dependence on the specific regularisation scheme. Our goal is to confront the new experimental data, in particular the triple-differential cross-section, to NLL-BFKL predictions in different schemes.

In Ref.[15], such a phenomenological investigation has been devoted to the proton structure function data, taking into account NLL-BFKL effects through an "effective kernel" (introduced in [12]) using three different schemes (denoted S3 and S4 from [11] and CCS from [12]). A saddle-point approximation for hard enough scales is used in order to obtain a phenomenological description of NLL-BFKL effects. In the present study devoted to forward-jet production, we implement them in a similar way, after taking into account the proper symmetric two-hard-scale feature of the forward-jet problem.

Some preliminary results were presented in [16], showing the potential of forward-jet data on $d\sigma/dx$ and specially $d\sigma/dxdk_T^2dQ^2$ to discuss NLL effects in the BFKL approach. In this paper, we present a detailed analysis of the NLL scheme and scale dependences and also discuss the sensitivity of our NLL-BFKL descriptions with respect to the photon impact factors. We also study the NLOQCD predictions, testing their relevance by comparing the use of different parton densities and differents renormalisation and factorisation scales.

The plan of the paper is the following. In section II, we present the phenomenological NLL-BFKL formulation of the forward-jet cross-sections for the three schemes S3, S4 and CCS, briefly mentioning the principles of its derivation. In section III, we compare the predictions of the 3 NLL-BFKL schemes to data, and also with LL-BFKL and NLOQCD predictions. We discuss the dependence of our results with respect to the choice of hard scale with which α_s is running in Section IV, and with respect to the assumption made for the photon impact factors in Section V. Section VI presents the scale and parton-density dependences of the NLOQCD predictions. Section VII is devoted to conclusions and outlook.

II. FORWARD-JET PRODUCTION IN THE BFKL FRAMEWORK

Forward-jet production in a lepton-proton collision is represented in Fig.1 with the different kinematic variables. We denote $\sqrt{s}$ the total energy of the lepton-proton collision and Q^2 the virtuality of the intermediate photon that undergoes the hadronic interaction. We shall use the usual kinematic variables of deep inelastic scattering: $x=Q^2/(Q^2+W^2)$ and $y=Q^2/(xs)$ where W is the center-of-mass energy of the photon-proton collision. In addition, $k_T \gg \Lambda_{QCD}$ is the jet transverse momentum and x_J its longitudinal momentum fraction with respect to the proton. The QCD cross-section for forward-jet production reads

$$\frac{d^{(4)}\sigma}{dxdQ^2dx_Jdk_T^2} = \frac{\alpha_{em}}{\pi x Q^2}\left\{\left(1-y+\frac{y^2}{2}\right)\frac{d\sigma_T^{\gamma^* p\to JX}}{dx_Jdk_T^2} + (1-y)\frac{d\sigma_L^{\gamma^* p\to JX}}{dx_Jdk_T^2}\right\} , \tag{1}$$

where $d\sigma_{T,L}^{\gamma^* p\to JX}/dx_Jdk_T^2$ is the cross-section for forward-jet production in the collision of the transversely (T) or longitudinally (L) polarized virtual photon with the target proton.

In the following, we consider the high-energy regime $x \ll 1$ in which the rapidity interval $Y=\log(x_J/x)$ is assumed to be very large. Following the phenomenological NLL-BFKL analysis of [15], one obtains for the forward-jet cross section:

$$\frac{d\sigma_{T,L}^{\gamma^* p\to JX}}{dx_Jdk_T^2} = \frac{\alpha_s(k_T^2)\alpha_s(Q^2)}{k_T^2Q^2}\; f_{eff}(x_J,k_T^2)\int\frac{d\gamma}{2i\pi}\left(\frac{Q^2}{k_T^2}\right)^{\gamma}\phi_{T,L}^{\gamma}(\gamma)\; e^{\bar{\alpha}(k_TQ)\chi_{eff}(\gamma,\bar{\alpha}(k_TQ))Y} \tag{2}$$

with the complex integral running along the imaginary axis from $1/2-i\infty$ to $1/2+i\infty$. The running coupling is

$$\bar{\alpha}(k^2) = \alpha_s(k^2)N_c/\pi = \left[b\log\left(k^2/\Lambda_{QCD}^2\right)\right]^{-1} , \qquad b=\frac{11N_c-2N_f}{12N_c} . \tag{3}$$

Some comments are in order.

- The NLL-BFKL effects are phenomenologically taken into account by the effective kernel $\chi_{eff}(\gamma,\bar{\alpha})$. The scheme-dependent NLL-BFKL kernels provided by the regularisation procedure $\chi_{NLL}(\gamma,\omega)$ depend on γ, the Mellin variable conjugate to Q^2/k_T^2 and ω, the Mellin variable conjugate to W^2/Qk_T. We shall consider the CCS scheme [12] and the S3 and S4 schemes [11] in which χ_{NLL} is supplemented by an explicit $\bar{\alpha}$ dependence. In

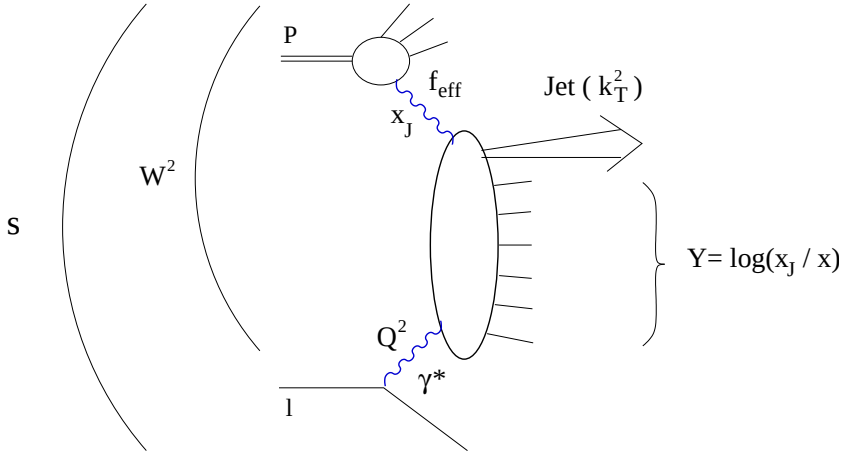

FIG. 1: Production of a forward jet in a lepton-proton collision. The kinematic variables of the problem are displayed. Q^2 is the virtuality of the photon that undergoes the hadronic interaction. s and W^2 are the total energies squared in the lepton-proton and photon-proton collisions respectively. k_T is the transverse momentum of the forward jet and x_J is its longitudinal momentum fraction with respect to the incident proton. Y is the rapidity interval between the two hard probes.

each case, the NLL kernels obey a *consistency condition* [11] which allows to reformulate the problem in terms of $\chi_{eff}(\gamma,\bar{\alpha})$. The effective kernel $\chi_{eff}(\gamma,\bar{\alpha})$ is obtained from the NLL kernel $\chi_{NLL}(\gamma,\omega)$ by solving the implicit equation:

$$\chi_{eff}(\gamma,\bar{\alpha}) = \chi_{NLL}(\gamma,\bar{\alpha}\ \chi_{eff}(\gamma,\bar{\alpha}))\ , \tag{4}$$

as a solution of the consistency condition.

Further details on the approximation (2) are given in Ref. [15], in particular regarding the definition of the three schemes (CCS, S3 and S4) which were studied for F_2, and that we will use for the forward-jet case. The only difference is that the kernel considered for F_2 was naturally the asymmetric one $\chi_{NLL}(\gamma+\omega/2,\omega)$. In the forward-jet problem, the energy scale is considered to be given symmetrically between the hard probes by $\log(W^2/k_TQ)$ instead of $\log(W^2/Q^2)\simeq\log(1/x)$ as was the case for F_2. In other words, we do not perform the shift $\gamma\to\gamma+\omega/2$ used for F_2.

- In formula (2), the renormalisation scale is $k^2=k_TQ$, in agreement with the energy scale [17]. In Section IV, we shall test the sensitivity of our results when using $k^2=\lambda\ k_TQ$ and varying λ. Following formula (4), the effective kernel is modified accordingly for each scheme, and we also modify the energy scale $k_TQ\to\lambda\ k_TQ$.

- It is important to note that in formula (2), we use the leading-order (Mellin-transformed) impact factors

$$\begin{pmatrix}\phi_T^\gamma(\gamma)\\ \phi_L^\gamma(\gamma)\end{pmatrix} = \pi\alpha_{em}N_c^2\sum_q e_q^2\frac{1}{2\gamma^2}\frac{\Gamma^3(1+\gamma)\Gamma^3(1-\gamma)}{\Gamma(2-2\gamma)\Gamma(2+2\gamma)(3-2\gamma)}\begin{pmatrix}(1+\gamma)(2-\gamma)\\ 2\gamma(1-\gamma)\end{pmatrix}\ . \tag{5}$$

for a transversely (T) and longitudinally (L) polarized virtual photon where e_f is the charge of the quark with flavor f. We consider massless quarks and sum over four flavors in (5). This is justified considering the rather high values of the photon virtuality ($Q^2>5$ GeV^2) used for the measurement. We point out that our phenomenological approach can be adapted to full NLL accuracy, once the next-leading impact factors are available. For completion, we shall discuss the sensitivity of our results with respect to typical next-leading modifications of $\phi_{T,L}^\gamma(\gamma)$ in Section V.

- In formula (2), $f_{eff}(x_J,k_T^2)$ is the effective parton distribution function and resums the leading logarithms $\log(k_T^2/\Lambda_{QCD}^2)$. It has the following expression

$$f_{eff}(x_J,k_T^2) = g(x_J,k_T^2) + \frac{C_F}{N_c}\big(q(x_J,k_T^2)+\bar{q}(x_J,k_T^2)\big)\ , \tag{6}$$

where g (resp. q, $\bar{q}$) is the gluon (resp. quark, antiquark) distribution function in the incident proton. Since the forward jet measurement involves perturbative values of k_T and moderate values of x_J, formula (2) features the collinear factorization of f_{eff}, with k_T^2 chosen as the factorization scale.

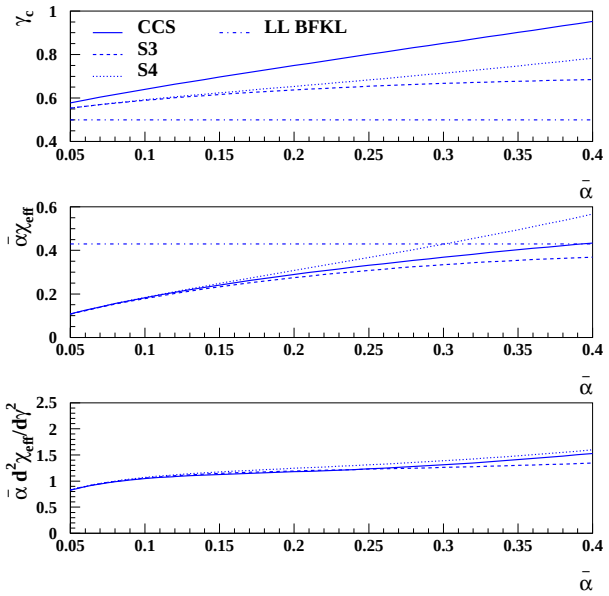

FIG. 2: γ_c, $\bar{\alpha}\chi_{eff}(\gamma_c,\bar{\alpha})$ and $\bar{\alpha}\chi''_{eff}(\gamma_c,\bar{\alpha})$, as functions of $\bar{\alpha}$ for the three BFKL resummation schemes CCS, S3 and S4. The fixed LL values are respectively 1/2, 0.43, and 5.47 (not shown on the figure) corresponding to $\bar{\alpha}=0.16$.

It is possible to estimate the complex integration in (2) using a saddle-point approximation in γ. In the BFKL regime we are working in, Y is very large, and the saddle-point equation

$$\frac{d\chi_{eff}}{d\gamma}(\gamma_c,\bar{\alpha}) = \chi'_{eff}(\gamma_c,\bar{\alpha}) = \frac{\log(k_T^2/Q^2)}{\bar{\alpha}Y} \tag{7}$$

becomes $\chi'_{eff}(\gamma_c,\bar{\alpha})=0$. Hence one finds for the theoretical forward-jet cross section

$$\frac{d\sigma_{T,L}^{\gamma^* p\to JX}}{dx_J dk_T^2} \simeq \frac{\alpha_s(k_T^2)\alpha_s(Q^2)}{k_T^2 Q^2} f_{eff}(x_J,k_T^2)\left(\frac{Q^2}{k_T^2}\right)^{\gamma_c} \frac{\phi^\gamma_{T,L}(\gamma_c)}{\sqrt{2\pi\bar{\alpha}\chi''_{eff}(\gamma_c,\bar{\alpha})\ Y}}\ \exp\left(\bar{\alpha}\chi_{eff}(\gamma_c,\bar{\alpha})Y - \frac{\log^2(Q^2/k_T^2)}{2\bar{\alpha}\chi''_{eff}(\gamma_c,\bar{\alpha})\ Y}\right), \tag{8}$$

where $\chi''_{eff}=d^2\chi_{eff}/d\gamma^2$. It is possible to extract the values of γ_c, $\bar{\alpha}\chi_{eff}(\gamma_c,\bar{\alpha})$ and $\bar{\alpha}\chi''_{eff}(\gamma_c,\bar{\alpha})$ after solving the implicit equation (4). They are given in Fig.2 for the different schemes, as functions of $\bar{\alpha}$ (for useful parametrizations, see Appendix I). The description of the forward-jet cross section is then almost parameter free; the value of $\bar{\alpha}(k_T Q)$ is imposed by the renormalisation group equations and only the overall normalisation is unknown (before knowing the next-leading impact factors for a full prediction).

By comparison, the LL-BFKL formula is formally the same as (8), with the substitutions

$$\chi_{eff}\to\chi_{LL}(\gamma)=2\psi(1)-\psi(1-\gamma)-\psi(\gamma)\ , \qquad \gamma_c\to 1/2\ , \qquad \bar{\alpha}(k^2)\to\bar{\alpha}=\text{const. parameter}\ , \tag{9}$$

where $\psi(\gamma)=d\log\Gamma(\gamma)/d\gamma$ is the logarithmic derivative of the Gamma function. One obtains

$$\left.\frac{d\sigma_{T,L}^{\gamma^* p\to JX}}{dx_J dk_T^2}\right|_{LL} \simeq \frac{\alpha_s(k_T^2)\alpha_s(Q^2)}{k_T^2 Q^2} f_{eff}(x_J,k_T^2)\ \frac{Q}{k_T}\ \frac{\phi^\gamma_{T,L}(1/2)}{\sqrt{2\pi\bar{\alpha}\chi''_{LL}(1/2)Y}}\ \exp\left(\bar{\alpha}\chi_{LL}(1/2)Y - \frac{\log^2(Q^2/k_T^2)}{2\bar{\alpha}\chi''_{LL}(1/2)Y}\right). \tag{10}$$

Inserting formula (8) (resp. (10)) into (1) gives the forward-jet cross-section in the NLL-BFKL (resp. LL-BFKL) energy regime. In the LL-BFKL case, this is a 2-parameter formula: the overall normalisation and $\bar{\alpha}$. In the NLL-BFKL case, the variables shown in Fig.2 are derived from the theory with running coupling constant, and are well-defined for each set of scales (Q^2,k_T^2). Hence, we deal with only one free parameter, the overall normalization. The interesting property of our phenomenological approach is that formula (2) has formally the structure of the LL formula, but with only one free parameter and a NLL kernel. The delicate aspect of the problem comes from the scheme-dependent effective kernel χ_{eff}.

III. NLL DESCRIPTION OF THE H1 DATA

The NLL-BFKL formula for the fully differential forward-jet cross section is obtained from (1) and (8). To compare the corresponding prediction with the data, one has to carry out a number of integrations over the kinematic variables. They have to be done while properly taking into account the kinematic cuts applied for the different measurements. The procedure is the same as the one described in Ref.[10], Appendix A. First one chooses the variables which lead to the weakest possible dependence of the differential cross section (we noticed that the best choice is $1/Q^2$, $1/k_T^2$, $\log(1/x_J)$, and $\log(1/x)$) and then the integrations are then computed numerically following the experimental cuts defined in Ref. [5, 6].

To fix the normalisation (the only free parameter) and check the quality of the data description using the BFKL formalism, we start by fitting the $d\sigma/dx$ H1 data [5]. The choice of this data set corresponds to the kinematical domain where the BFKL formalism is expected to hold ($x \ll 1$ and $Q^2/k_T^2 \sim 1$). We then use the relative normalisations obtained between the different NLL BFKL calculations (CCS, S3 and S4) to make predictions for the triple differential cross section $d\sigma/dx dk_T^2 dQ^2$. For this first analysis, the coupling $\bar{\alpha}$ is running with the scale $k_T Q$ and we used $\gamma_c = 1/2$ in the photon impact factors.

A. The cross-section $d\sigma/dx$

We considered two kinds of fits: the first one is performed using statistical and systematics errors and the second one with statistical errors only. The systematics errors are very much point to point correlated, and this is why it is important to perform the fits with statistical errors only. Ideally, one should use the statistical errors added in quadrature with the uncorrelated ones but this information is not available.

The fit results to the $d\sigma/dx$ H1 data are given in Table I. The χ^2 values of the fits performed using the full (statistical and systematics) errors are quite good, always less than 1, for the three NLL-BFKL schemes we considered. This shows the possibility of describing the forward jet cross section using the BFKL NLL formalism. The fits using statistical errors only (which assume implicitely that the systematics are maximally correlated which is close to reality) show interesting features. The S4 fit can describe the data nicely ($\chi^2 = 5.6/5$ d.o.f.) whereas the S3 and CCS schemes show higher values of χ^2 ($\chi^2 = 45.9/5$ and $\chi^2 = 20.4/5$ respectively). This indicates that the S4 scheme is favored.

The curves corresponding to the fit with statistical errors only are displayed in Fig.3, left plot. Although this will be discussed in more details in Section IV, we also display the results obtained for the S4 scheme when varying the renormalisation scale in the range $[k_T Q/\lambda, \lambda\ k_T Q]$ with $\lambda = 2$. We notice that this change of scale essentially affects the overall normalisation and thus does not alter the quality of the fit, after reajusting the normalisation.

A comparison of the S4 fit with the LL-BFKL results taken from Ref. [10] is shown in Fig.3, right plot. We notice the tiny difference between the LL and NLL results (the corresponding curves are not distinguishable on the figure). This confirms that the data are consistent with the BFKL enhancement towards small values of x. Contrary to the proton structure function F_2, the forward-jet cross section $d\sigma/dx$ does not show large NLL-BFKL corrections, once the overall normalisation fitted. This is due to the rather small value of the coupling $\bar{\alpha} \simeq 0.16$ obtained in the LL-BFKL fit [10], corresponding to an unphysically large effective scale.

We also present in Fig.3 the fixed order QCD calculation based on the DGLAP evolution of parton densities. The next-to-leading order (NLO) prediction of forward-jet cross sections is obtained using the NLOJET++ generator [19]. CTEQ6.1M [20] parton densities were used, and the renormalization μ_r and the factorization scale μ_f were set equal to $\mu_r^2 = \mu_f^2 = Q k_t^{max}$, where k_t^{max} corresponds to the maximal transverse momentum of forward jets in the event. The NLOQCD predictions do not describe the data at small values of x, as they are below by a factor of order 2.

scheme	fit	χ^2/dof	N
CCS	stat. + syst.	0.90/5	0.1332 ± 0.0074
CCS	stat. only	22.2/4	0.1367 ± 0.0016 ± 0.0170
S3	stat. + syst.	1.74/5	0.1514 ± 0.0085
S3	stat. only	46.5/5	0.1576 ± 0.0018 ± 0.0196
S4	stat. + syst.	0.29/5	0.1094 ± 0.0061
S4	stat. only	5.4/5	0.1096 ± 0.0013 ± 0.0137

TABLE I: Results of the NLL-BFKL fits to the H1 $d\sigma/dx$ data. The relative values between the different overall normalisations N can be compared.

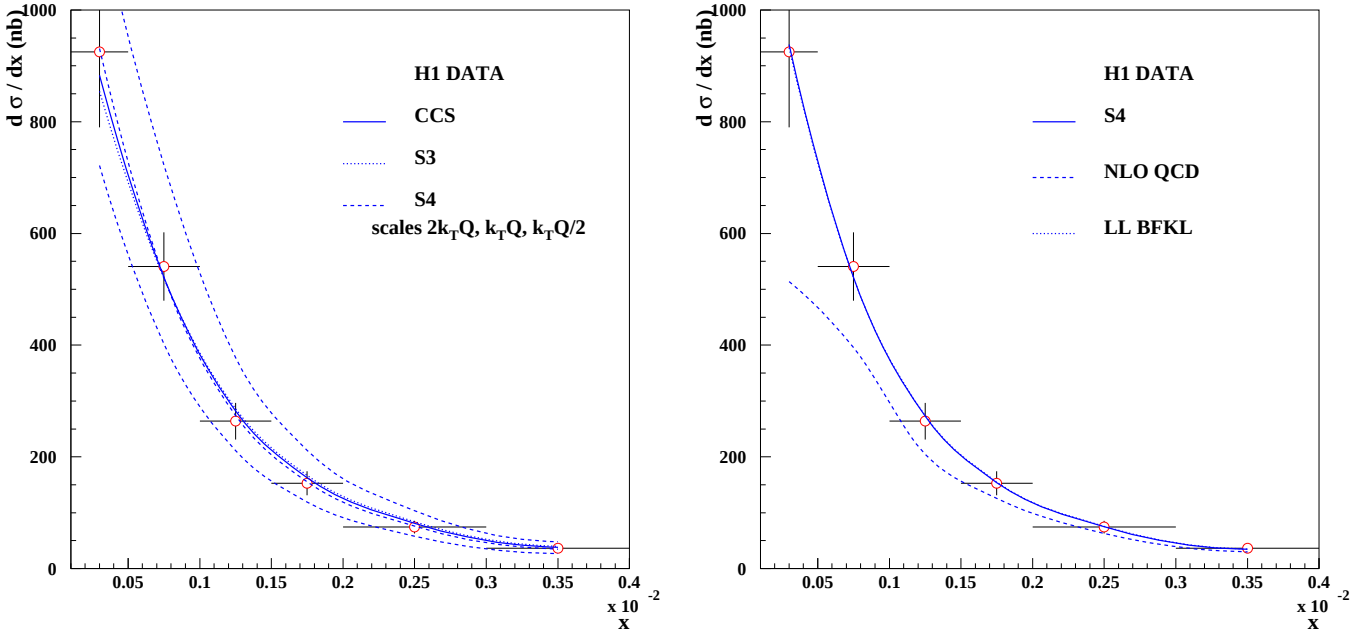

FIG. 3: The forward-jet cross-section $d\sigma/dx$ measured by the H1 collaboration. Left plot: comparison with the three NLL-BFKL parametrizations S4, CCS and S3 using the $k_T Q$ scale. For the S4 scheme, we also display the results of the $2k_T Q$ and $k_T Q/2$ scales without changing the normalisation; the considered range of renormalisation scale for S4 does not alter the quality of the fit, after reajusting the normalisation. Right plot: comparison with the LL and NLL (S4) BFKL fits and with NLOQCD predictions. We see a good agreement between the data and the BFKL fits, the NLL-BFKL S4 fit and the LL-BFKL fit are not distinguishable on the figure. The NLOQCD predictions do not describe the data.

The sensitivity of these predictions with respect to variations of the renormalization and factorization scales will be discussed in Section VI, as well as their dependence when using other parton densities.

The fit parameters obtained with statistical error only will be used in the following to make predictions for other observables, namely the triple differential cross section $d\sigma/dxdk_T^2dQ^2$. The value of $\bar{\alpha}$ for the LL-BFKL fit will be kept as well as the relative normalisation between the different NLL-BFKL calculations (CCS, S3 and S4).

B. The triple differential cross-section $d\sigma/dxdk_T^2dQ^2$

The triple differential cross section $d\sigma/dxdk_T^2dQ^2$ is an interesting observable as it has been measured with 3 different k_T^2 and Q^2 cuts, yielding 9 different regions for the ratio $r = k_T^2/Q^2$. It was noticed in [10] that the LL-BFKL formalism leads to a good description of the data when r is close to 1 and deviates from the data when r is further away from 1, as effects due to the ordering between Q and k_T start to set in. NLOQCD predictions show the reverse trend.

The H1 data for $d\sigma/dxdk_T^2dQ^2$ are shown in Fig.4. The upper plot shows the comparison with the S4 prediction, the LL-BFKL results (taken directly from [10]) and NLOQCD predictions. It is quite remarkable that the NLL-BFKL calculation, which includes some ordering between Q and k_T, leads to a good description of the H1 data on the full range. As it was the case for $d\sigma/dx$, the difference between the LL and NLL results is small when $r \sim 1$. By contrast when r differs from 1, the difference is significant, and the observable $d\sigma/dxdk_T^2dQ^2$ is quite sensitive to NLL-BFKL effects.

As a result, the best overall descrition of the data is obtained with the NLL-BFKL formalism. The lower plot of Fig.4 shows the comparison between the H1 data and the predictions of the different NLL schemes. Although the description is good in all cases, the predictions of the S3 and CCS schemes do not compare with the data as well as the predictions of the S4 scheme, which is therefore favored. This will be confirmed by the analysis of Section V.

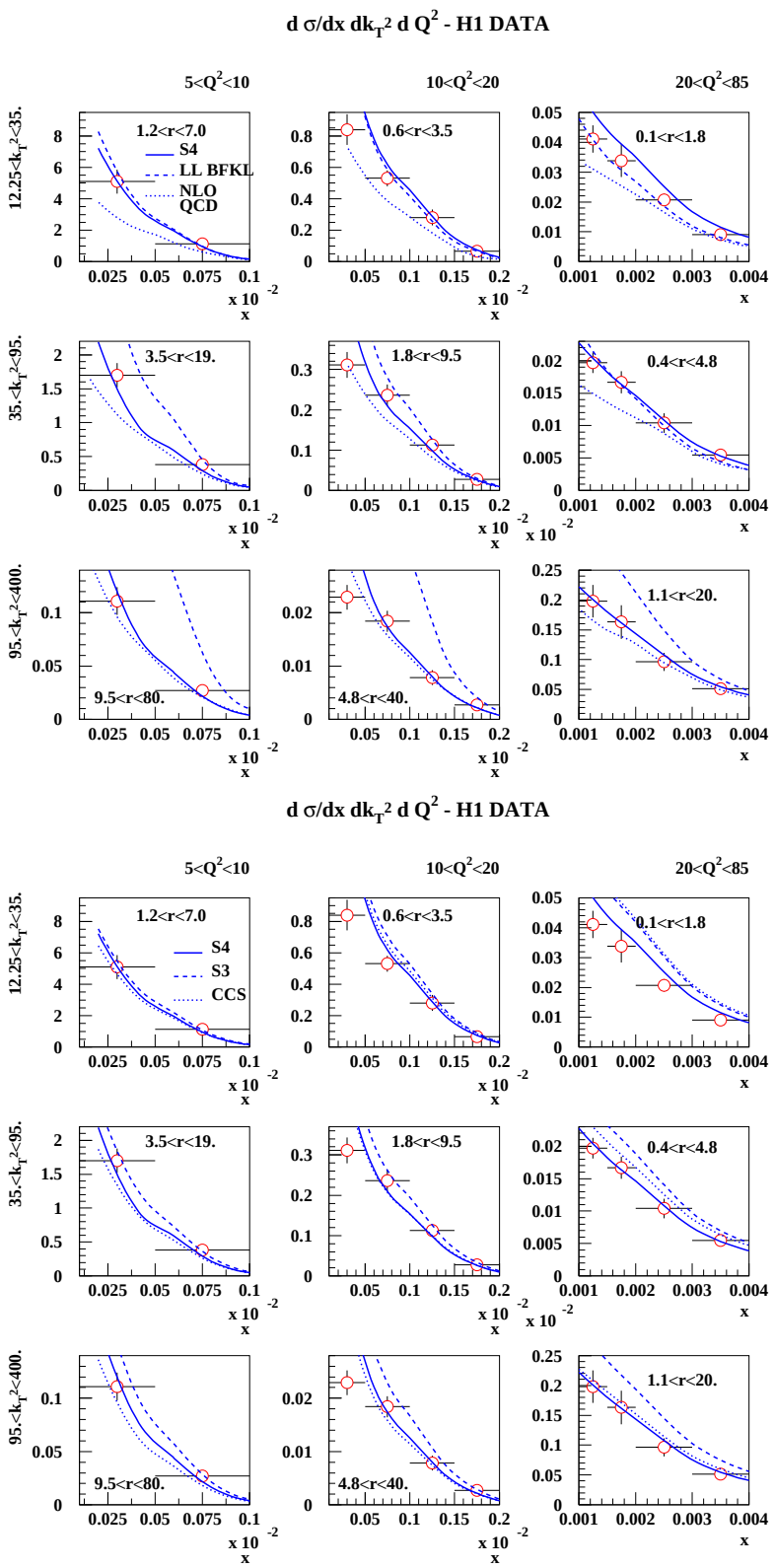

FIG. 4: The forward-jet cross-section $d\sigma/dxdQ^2dk_T^2$ measured by the H1 collaboration. Upper plot: the data are compared with the LL and NLL (S4) BFKL fits and with NLOQCD predictions. The best description of the data over the whole kinematic range is obtained by the NLL-BFKL approach. Lower plot: the data are compared to the three NLL-BFKL predictions (CCS, S3 and S4). The S4 scheme is favored

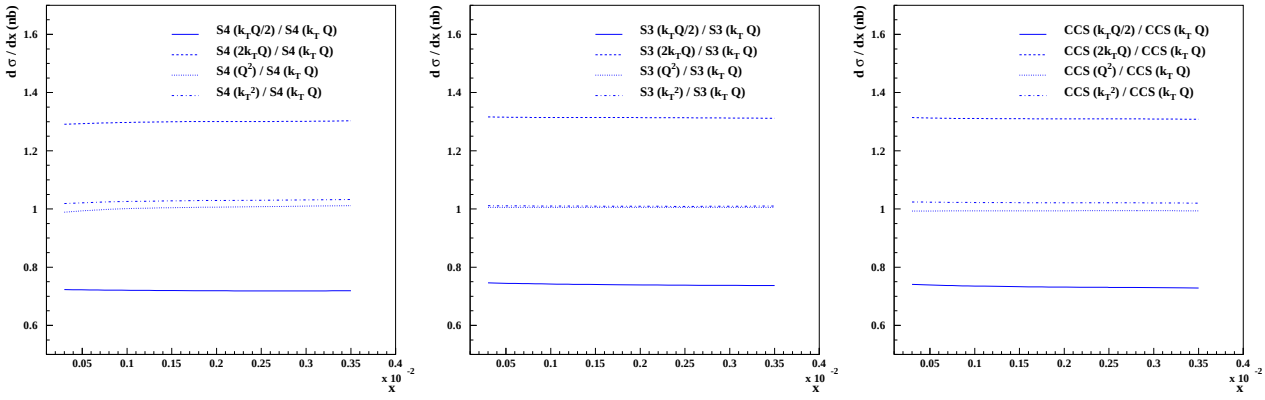

FIG. 5: Renormalisation scale dependence for the S4, S3 and CCS schemes, with the scale $k_T Q$ chosen as the reference. The change of scale essentially affects the overall normalisation and thus does not alter the quality of the fits.

IV. RENORMALISATION SCALE DEPENDENCE OF THE NLL DESCRIPTION

In this section, we study the renormalisation scale dependence of the NLL-BFKL description. In the previous section, the choice was $k^2 = k_T Q$ and we now test the sensitivity of our results when using $k^2 = \lambda\ k_T Q$ in the following four cases: $\lambda = 2$, $\lambda = 1/2$, $\lambda = k_T/Q$, and $\lambda = (Q/k_T)$. We use formula (2) with the appropriate substitution [18]

$$\bar{\alpha}(k_T Q) \rightarrow \bar{\alpha}(\lambda k_T Q) + b\ \bar{\alpha}^2(k_T Q) \log(\lambda) \tag{11}$$

and with the effective kernel modified accordingly following formula (4). We also modify the energy scale $k_T Q \rightarrow \lambda\, k_T Q$.

We first study the case of $d\sigma/dx$. The results obtained when using $\lambda = 2^{\pm 1}$ for the S4 scheme were already shown in Fig.3. In this section, we display the results in terms of ratios with the prediction of the $k_T Q$ scale chosen as the reference. The results for the different scales are shown in Fig.5 for each NLL-BFKL scheme.

When $\lambda = (k_T/Q)^{\pm 1}$, the ratio is very close to one, showing tiny differences. This is due the cut on k_T^2/Q^2 close to 1 used to measure the observable $d\sigma/dx$. When $\lambda = 2^{\pm 1}$, the differences are significantly bigger. However in any case, the change of scale essentially affects the overall normalisation and thus does not alter the quality of the fits, after reajusting the normalisation. This is confirmed by the results of Table II, which presents new fits performed to the $d\sigma/dx$ data for each different scale: for each scheme, the χ^2 values are almost insensitive to the scale. Note that, for larger values of λ such as $\lambda = 4$, the quality of the fit deteriorates due to the large values reached by $\bar{\alpha}$ in the non-perturbative range.

The next step is to study the effect of the renormalisation-scale dependence on the triple differential cross section, applying the relative normalisations of Table II while computing the corresponding predictions. The results for the S4 scheme are shown in Fig.6 and the scale dependence is generally found to be small. The biggest effect yields an uncertainty of about the same magnitude as the experimental errors and it is obtained for $\lambda = (k_T/Q)^{\pm 1}$ and for large values of $r = k_T^2/Q^2$ (see upper plot). For $\lambda = 2^{\pm 1}$, the differences are significantly smaller (see lower plot). The conclusion is identical in the case of the S3 and CCS schemes and the corresponding results are displayed in Appendix II (S3: Fig.11, CCS:Fig.12).

	Scale	χ^2/dof	N
S4	$k_T Q$	5.4/5	0.1096 ± 0.0013
	$2k_T Q$	5.5/5	0.1420 ± 0.0016
	$k_T Q/2$	5.8/5	0.0791 ± 0.0009
	Q^2	5.4/5	0.1099 ± 0.0013
	k_T^2	5.4/5	0.1071 ± 0.0012

	Scale	χ^2/dof	N
S3	$k_T Q$	46.5/5	0.1576 ± 0.0018
	$2k_T Q$	45.8/5	0.2072 ± 0.0024
	$k_T Q/2$	42.3/5	0.1170 ± 0.0013
	Q^2	46.4/5	0.1567 ± 0.0018
	k_T^2	45.7/5	0.1560 ± 0.0018

	Scale	χ^2/dof	N
CCS	$k_T Q$	22.2/5	0.1367 ± 0.0016
	$2k_T Q$	21.2/5	0.1793 ± 0.0020
	$k_T Q/2$	18.5/5	0.1006 ± 0.0011
	Q^2	22.4/5	0.1377 ± 0.0016
	k_T^2	21.2/5	0.1337 ± 0.0015

TABLE II: Impact on the fits to the H1 $d\sigma/dx$ data for each NLL-BFKL scheme when using different renormalisation scales.

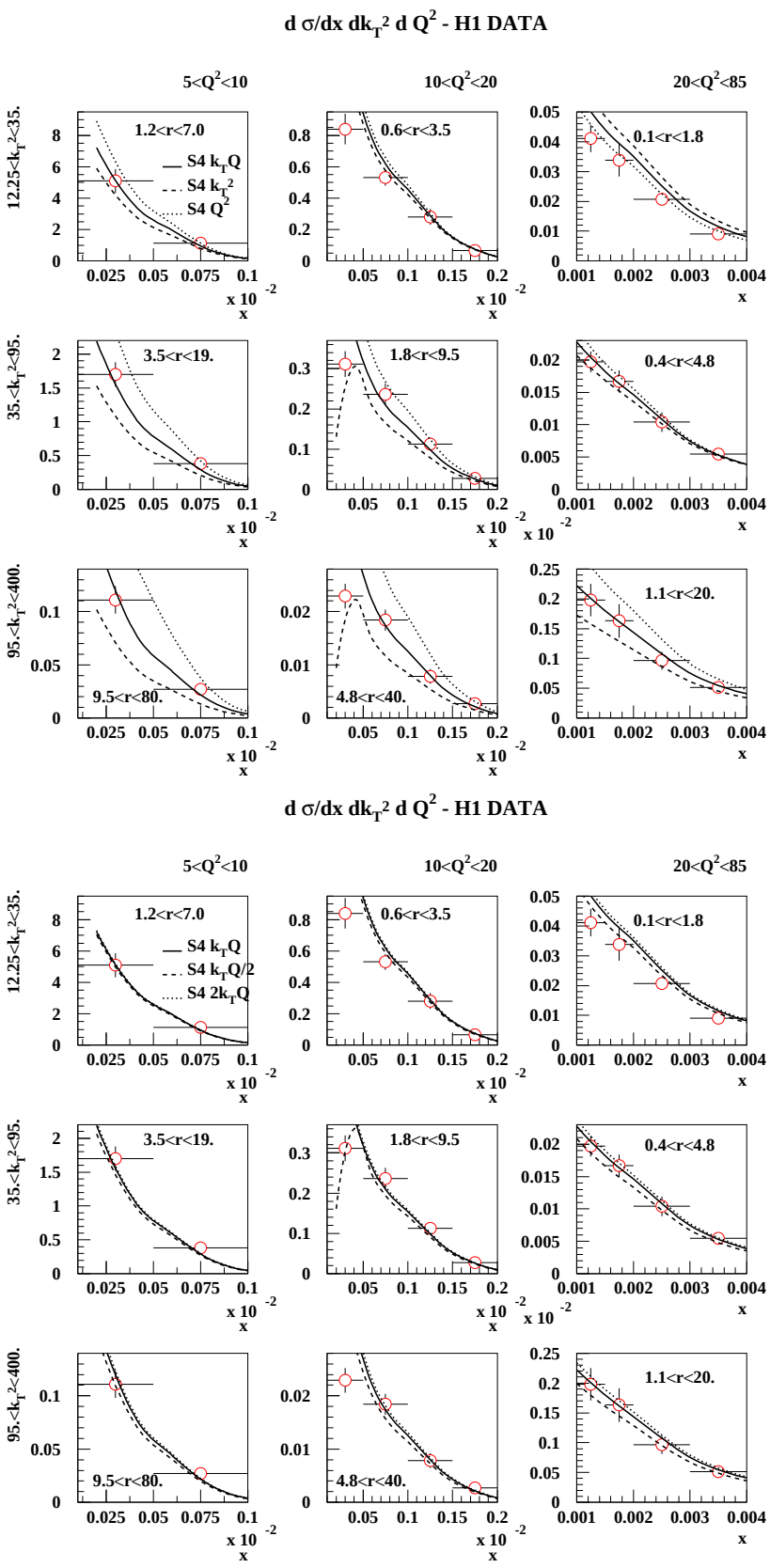

FIG. 6: Renormalisation-scale variation effects on the triple differential cross section for the S4 scheme. The relative normalisations coming from the $d\sigma/dx$ fits has been applied. Upper plot: $\lambda = (k_T/Q)^{\pm 1}$. Lower plot: $\lambda = 2^{\pm 1}$.

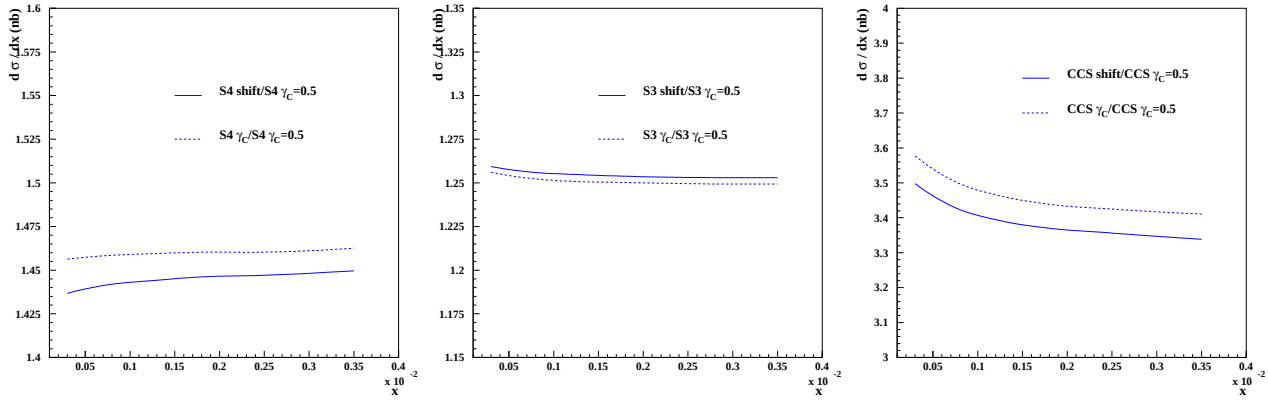

FIG. 7: Impact factor dependence for the S4, S3 and CCS schemes, with the case $\gamma_c = 1/2$ chosen as the reference. For the S4 and S3 schemes, the change of scale essentially affects the overall normalisation and thus does not alter the quality of the fits. By contrast for the CCS scheme, the χ^2 values are sensitive to modifications of the impact factor.

V. IMPACT FACTOR DEPENDENCE OF THE NLL DESCRIPTION

In this section, we study the dependence of our results with respect to typical next-leading modifications of the impact factors. Indeed, since the next-leading impact factors are unknown, it is useful to see if our results are stable for different possible modifications. From (1) and (2) one notes that the impact factors are involved in the computation of the fully differential cross-section via the following factor in the integrand:

$$(1 - y + y^2/2)\phi_T^\gamma(\gamma) + (1 - y)\phi_L^\gamma(\gamma) \ . \tag{12}$$

In the previous section, the impact factors ϕ_T^γ and ϕ_L^γ were computed by default at $\gamma \equiv \gamma_c = 1/2$ and we now test the sensitivity of our results when using other prescriptions.

A natural idea is to compute the impact factors at γ_c where γ_c is the genuine solution to the saddle point equation $\chi'_{eff}(\gamma_c, \bar{\alpha}) = 0$. We also tried a third prescription by computing the impact factors at γ_c and multiplying (12) with the factor $(k_T/Q)^{\bar{\alpha}\chi_{eff}(\gamma_c,\bar{\alpha})}$. This is equivalent to performing the shift $\gamma \to \gamma + \omega/2$ used for the F_2 analysis [15].

We display the results in terms of ratios with the prediction of the $\gamma_c = 1/2$ case scale chosen as the reference. The results for the different prescriptions are shown in Fig.7 for each NLL-BFKL scheme. We notice that the differences in normalisation are found to be relatively large with ratios of the order of 1.45, 1.25 and 3.5 for the S4, S3 and CCS schemes respectively. However, as indicated in Table III, the fit quality is not changed except for the CCS scheme which is less stable (but slightly improved).

After applying the differences in normalisation, it is possible to compare the effect of the different impact factors on the triple differential cross section. The results are given in Fig.8 and Fig.9. While the difference is found to be small for the S3 and S4 schemes, the CCS scheme is not stable with respect to the modifications of the impact factors.

Scheme	Impact factor	χ^2/dof	N
S4	$\gamma_c = 0.5$	5.4/5	0.1096 ± 0.0013
	γ_c	5.5/5	0.0751 ± 0.0009
	$shift$	5.4/5	0.0760 ± 0.0009
S3	$\gamma_c = 0.5$	46.5/5	0.1576 ± 0.0018
	γ_c	44.2/5	0.1258 ±0.0014
	$shift$	44.5/5	0.1254 ± 0.0014
CCS	$\gamma_c = 0.5$	22.2/5	0.1367 ± 0.0016
	γ_c	12.0/5	0.0390 ± 0.0004
	$shift$	12.4/5	0.0399 ± 0.0005

TABLE III: Impact on the fits to the H1 $d\sigma/dx$ data for each NLL-BFKL scheme when using different modifications of the impact factors.

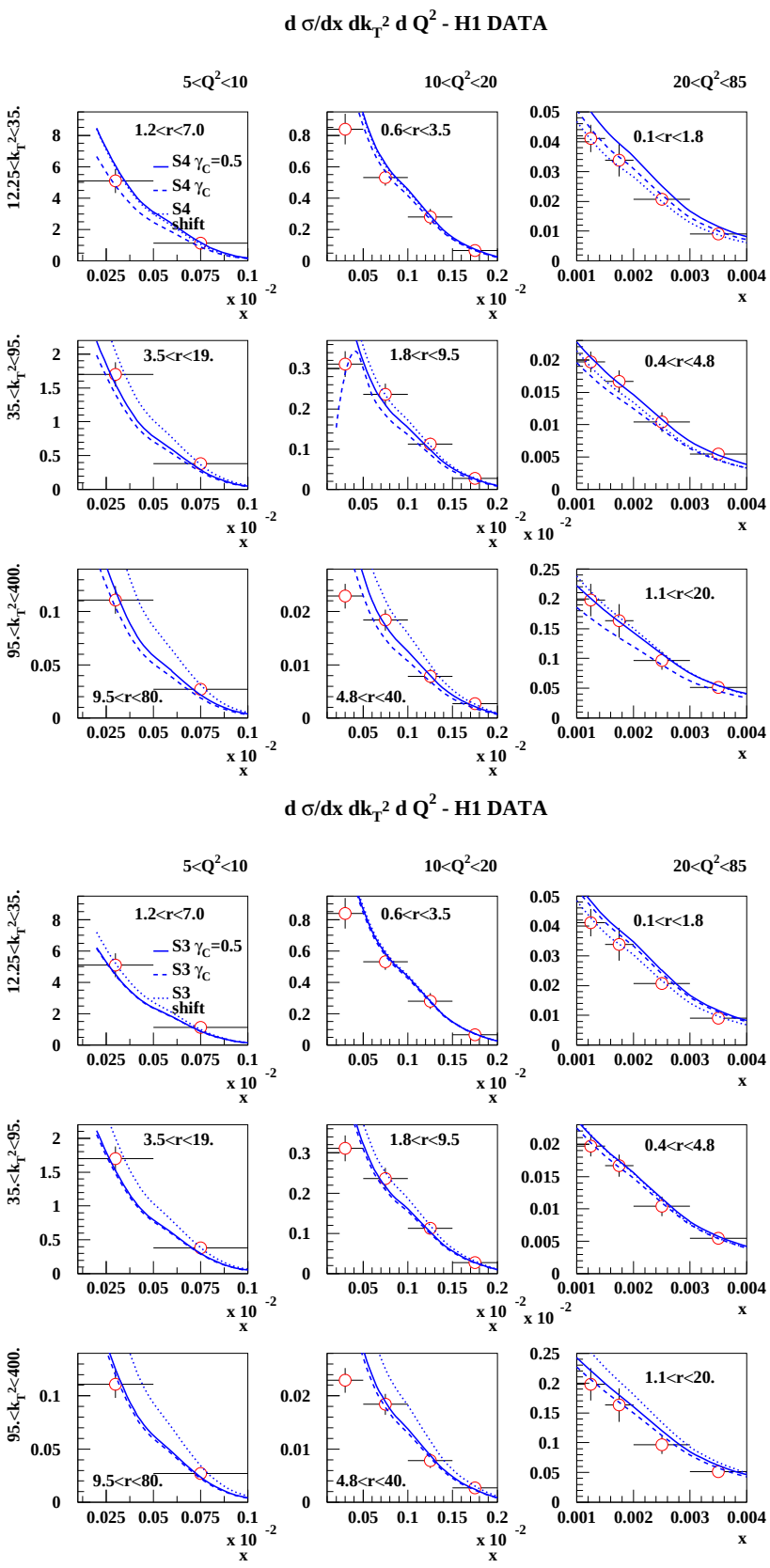

FIG. 8: Impact factor dependence of the triple differential cross section. The relative normalisations coming from the $d\sigma/dx$ fits has been applied. Upper plot: S4. Lower plot: S3.

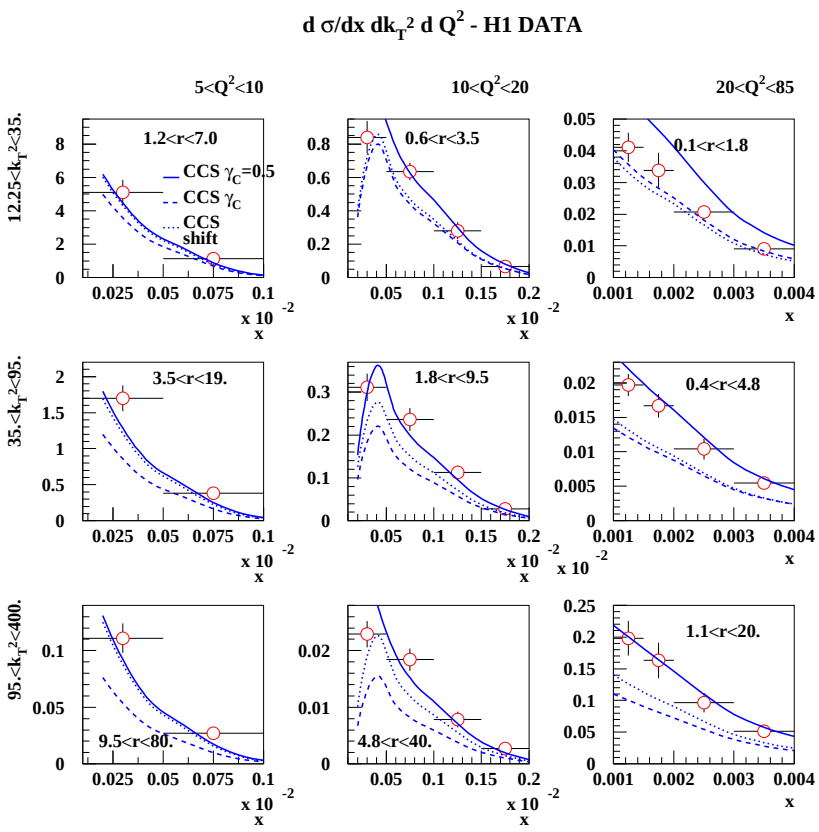

FIG. 9: The same as Fig.8 for the CCS scheme.

VI. PDF AND SCALE DEPENDENCE OF THE NLOQCD PREDICTIONS

To obtain the NLOQCD predictions of the forward-jet data, the photon-parton hard cross section is computed at next-to-leading order with respect to α_s, and the leading and next-leading logarithms $\alpha_s^n \log^n Q^2$ and $\alpha_s^n \log^{n-1} Q^2$ are resummed using the DGLAP equations [3] which govern the evolution of the parton distribution functions (PDFs) of the proton.

The prediction for the forward jet cross section at next-to-leading order is calculated using NLOJET++ [19]. The renormalisation scale μ_r^2 and the factorisation scale μ_f^2 were chosen as $\mu_r^2 = \mu_f^2 = Qk_T^{max}$, where k_T^{max} denotes the maximal transverse momentum of forward jets in the event. To obtain the uncertainty associated with the scale choice, we varied the scales in the conventional range $Qk_T^{max}/4 < \mu_r^2 = \mu_f^2 < 4Qk_T^{max}$. Another scale choice $\mu_r^2 = \mu_f^2 = k_T^{max2}$ was also tested; however, it yielded a result located within the mentioned scale uncertainty bounds and thus shall not be considered further. We point out that the scale uncertainty is rather large in the low x regime. This is due to the large NLO correction suggesting that higher order corrections might be significant.

An additional contribution to the total uncertainty of the calculation is due to the choice of the PDFs of the proton. Throughout the calculation, we use the CTEQ6.1M PDF parametrization which provides not only the central PDF S_0 corresponding to the best fit to data, but also additional 40 distribution functions S_i^+, S_i^-, $i = 1 \ldots 20$ devoted for uncertainty studies [20]. The total PDF uncertainty ΔX of the observable X is than computed as

$$(\Delta X)^2 = \sum_{i=1}^{20} \left[\frac{X(S_i^+) - X(S_i^-)}{2} \right]^2 . \tag{13}$$

We noticed that the main contribution to the PDF uncertainty comes from the gluon PDF.

The DGLAP calculation of the $d\sigma/dx$ distribution measured by H1 is presented in Fig.10, upper plot. This approach clearly fails to describe the data for the low values of x. In comparision with Fig.3 and Fig.4, we see that $d\sigma/dx$ is more sensitive to the BFKL dynamics than the triple differential distribution as the deviation from data is eminent.

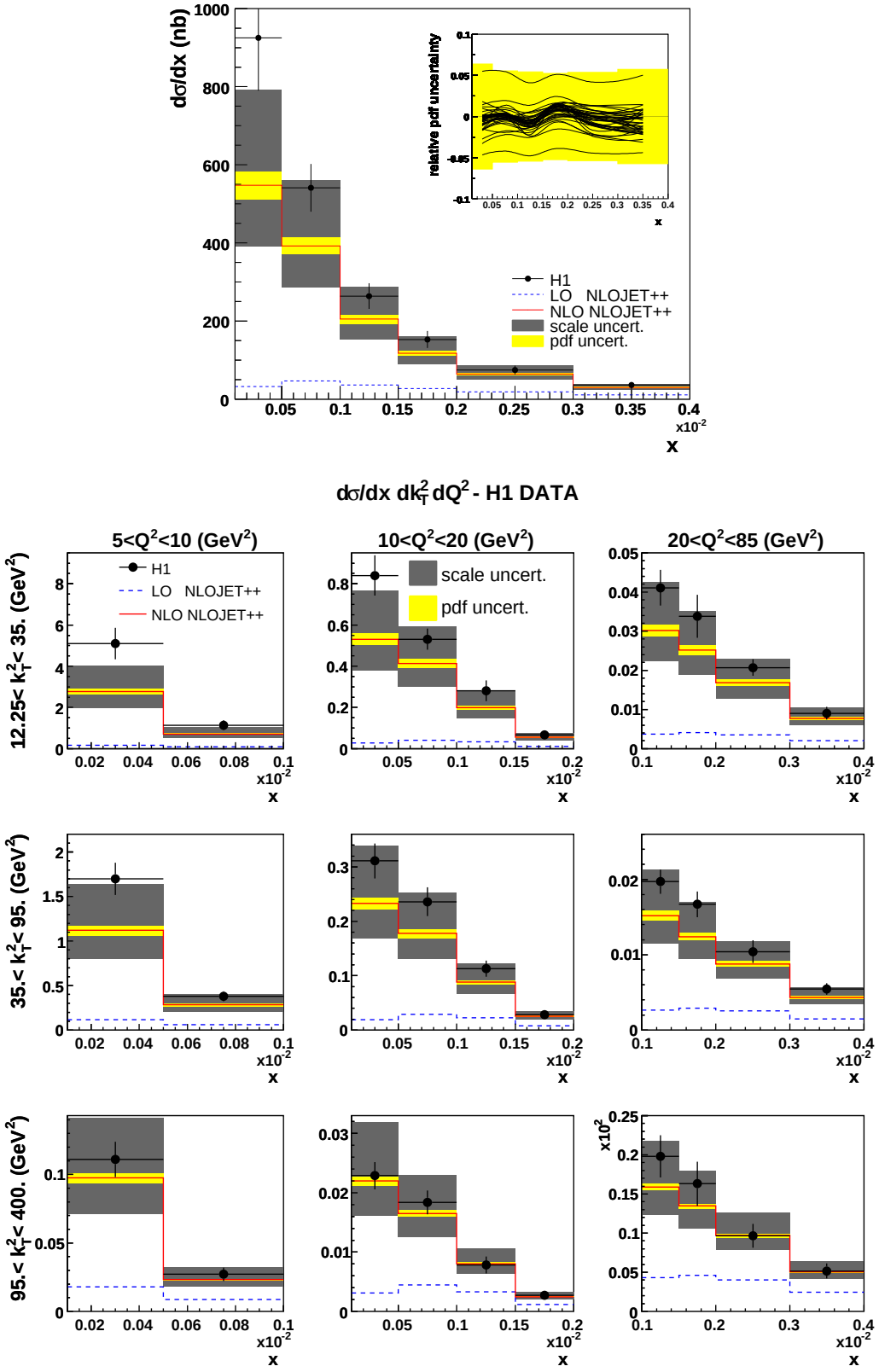

FIG. 10: Upper plot: scale and PDF uncertainties of the $d\sigma/dx$ distribution; the particular contributions of different 40 PDFs from CTEQ6.1M to the total PDF uncertainty (yellow area) is depicted in the inset. Lower plot: scale and PDF uncertainties for the triple differential distribution $d\sigma/dxdQ^2dk_T^2$. In both cases, the scales varied in the range $0.25\ Qk_T^{max} < \mu_r^2 = \mu_f^2 < 4\ Qk_T^{max}$ are displayed (shaded gray area).

The PDF uncertainty study is shown in the inset. The solid lines represent a ratio of the cross section calculated with various PDFs S_i^+, S_i^-, normalized to the cross section calculated with the central PDF S_0. The gluon PDF (i=15) has the greatest impact on the uncertainty and other PDFs can be neglected. The uncertainty study of $d\sigma/dxdk_T^2dQ^2$ is shown in Fig.10, lower plot. The PDF uncertainty was obtained taking into account the gluon density (which practically dictates the overall PDF uncertainty) only.

The main conclusion which can be drawn from Fig.10 is that at low values of x, the NLOQCD results suffer from large uncertainties, and indicate that NNLO calculations are needed to obtain genuine predictions in this framework.

VII. CONCLUSION

We performed a phemomenological analysis of the H1 forward-jet data, looking for effects of next-to-leading logarithms in the BFKL approach. Let us briefly summarize our results.

- For the cross section $d\sigma/dx$, measured in the kinematical regime $Q^2/k_T^2 \sim 1$, we obtain a good description of the H1 data by NLL-BFKL predictions (see Table I and Fig.3a). In addition, the difference between the LL-BFKL and NLL-BFKL descriptions is very small once the overall normalisation fitted (see Fig.3b). This confirms the validity of the BFKL description of [8, 10] previously obtained with the LL formula and a rather small effective coupling.

- In the case of the triple differential cross section $d\sigma/dxdk_T^2dQ^2$, the same conclusions holds when $r = k_T^2/Q^2 \sim 1$. In addition when r differs from 1, the NLL-BFKL description is quite different from the LL-BFKL one, as it is closer to the NLOQCD calculation. As a result, the best overall descrition of the data for $d\sigma/dxdk_T^2dQ^2$ is obtained with the NLL-BFKL formalism (see Fig.4).

- The renormalisation scale dependence of our results has been thoroughly studied and we showed the stability of the NLL-BFKL approach when using the scales k_TQ, $2k_TQ$, $k_TQ/2$, k_T^2, and Q^2. For $d\sigma/dx$, the change of scale essentially affects the overall normalisation and does not alter the quality of the fits (see Table II and Fig.5). For $d\sigma/dxdk_T^2dQ^2$, the biggest effect yields an uncertainty of about the same magnitude as the experimental errors (see Fig.6).

- We want to stress that the HERA data allow for a detailed study of the NLL-BFKL approach and of the QCD dynamics of forward jets. In particular, it has the potential to address the question of the remaining ambiguity corresponding to the dependence on the specific regularisation scheme of the NLL kernel. For instance, the predictions of the CCS and S3 schemes do not compare with the data as well as the predictions of the S4 scheme, as indicated by the χ^2 values given in Table I and by the comparison shown in Fig 4b.

- Our analysis is to be completed with the next-leading photon impact factors, when available. However we tested the stability of our approach when implementing typical next-leading modifications of leading-order impact factors. The results show some sensitivity (see Table III and Fig.7-9), especially for the CCS scheme. This indicates that, when the next-leading impact factors will be known, the predictions between different schemes could differ significantly, allowing for a strong test of NLL-BFKL predictions.

- Finally, we computed the NLOQCD predictions using the NLOJET++ generator and CTEQ6.1M [20] parton densities. We tested their relevance by comparing the use of different parton densities and renormalisation and factorisation scales (see Fig.10). The NLOQCD predictions do not describe the data at small values of x, and they suffer from large uncertainties, showing the need for higher-order corrections.

Forward-jet production is the first observable for which the NLL-BFKL description works while the standard NLOQCD does not work. We need the complete knowledge of the next-leading impact factors before drawing final conclusions, but our analysis strongly suggests that the data show the BFKL enhancement at small values of x. This is of great interest in view of the LHC, where similar QCD dynamics will be tested with Mueller-Navelet jets [21, 22].

Acknowledgments

We would like to thank Laurent Schoeffel and Sebastian Sapeta for providing their numerical evaluations of the effective kernel. This research was supported in part by RIKEN, Brookhaven National Laboratory and the U.S. Department of Energy [DE-AC02-98CH10886].

APPENDIX I: Expressions for γ_c, $\bar{\alpha}\chi_{eff}(\gamma_c,\bar{\alpha})$ and $\bar{\alpha}\chi''_{eff}(\gamma_c,\bar{\alpha})$, as functions of $\bar{\alpha}$.

The effective kernel used for F_2 in [15] is obtained by solving the implicit equation

$$\tilde{\chi}_{eff} = \tilde{\chi}_{NLL}(\gamma, \bar{\alpha}\ \tilde{\chi}_{eff})\ , \tag{14}$$

with the NLL kernel defined as

$$\tilde{\chi}_{NLL}(\gamma,\omega) = \chi_{NLL}(\gamma+\omega/2,\omega)\ . \tag{15}$$

In terms of $\tilde{\chi}_{eff}$, formula (8) can be rewritten

$$\frac{d\sigma^{\gamma^* p\to JX}_{T,L}}{dx_J dk_T^2} \simeq \frac{\alpha_s(k_T^2)\alpha_s(Q^2)}{k_T^2 Q^2} f_{eff}(x_J,k_T^2)\ \left(\frac{Q^2}{k_T^2}\right)^{\tilde{\gamma}_c} \frac{\phi^{\gamma}_{T,L}(\tilde{\gamma}_c+\bar{\alpha}\tilde{\chi}_{eff}(\tilde{\gamma}_c,\bar{\alpha})/2)}{\sqrt{2\pi\bar{\alpha}\tilde{\chi}''_{eff}(\tilde{\gamma}_c,\bar{\alpha})\ [Y+\log(Q/k_T)]}}$$
$$\exp\left(\bar{\alpha}\tilde{\chi}_{eff}(\tilde{\gamma}_c,\bar{\alpha})[Y+\log(Q/k_T)] - \frac{\log^2(Q^2/k_T^2)}{2\bar{\alpha}\tilde{\chi}''_{eff}(\tilde{\gamma}_c,\bar{\alpha})\ [Y+\log(Q/k_T)]}\right)\ , \tag{16}$$

with $\tilde{\gamma}_c$ solution of $\tilde{\chi}'_{eff}(\tilde{\gamma}_c,\bar{\alpha})=0$. The functions represented in Fig.2 are actually $\tilde{\gamma}_c$, $\bar{\alpha}\tilde{\chi}_{eff}(\tilde{\gamma}_c,\bar{\alpha})$ and $\bar{\alpha}\tilde{\chi}''_{eff}(\tilde{\gamma}_c,\bar{\alpha})$. The parametrizations are all of the same form:

$$\begin{pmatrix} \tilde{\gamma}_c \\ \bar{\alpha}\tilde{\chi}_{eff}(\tilde{\gamma}_c,\bar{\alpha}) \\ \bar{\alpha}\tilde{\chi}''_{eff}(\tilde{\gamma}_c,\bar{\alpha}) \end{pmatrix} = A + B\bar{\alpha} + C\bar{\alpha}^2 + D\bar{\alpha}^3 + E\bar{\alpha}^4 \tag{17}$$

and the values of the parameters A, B, C, D and E are given in Table II

scheme	formula	A	B	C	D	E
CCS	$\tilde{\gamma}_c$	0.507	1.535	-2.561	5.675	-4.806
	$\bar{\alpha}\tilde{\chi}_{eff}(\tilde{\gamma}_c,\bar{\alpha})$	0.013	2.166	-5.760	10.85	-8.535
	$\bar{\alpha}\tilde{\chi}''_{eff}(\tilde{\gamma}_c,\bar{\alpha})$	0.427	11.012	-64.26	171.2	-155.7
S3	$\tilde{\gamma}_c$	0.507	1.074	-2.980	5.195	-4.206
	$\bar{\alpha}\tilde{\chi}_{eff}(\tilde{\gamma}_c,\bar{\alpha})$	0.014	2.147	-5.958	10.38	-8.402
	$\bar{\alpha}\tilde{\chi}''_{eff}(\tilde{\gamma}_c,\bar{\alpha})$	0.436	10.659	-57.95	144.0	-129.0
S4	$\tilde{\gamma}_c$	0.507	1.059	-2.725	6.442	-4.835
	$\bar{\alpha}\tilde{\chi}_{eff}(\tilde{\gamma}_c,\bar{\alpha})$	0.015	2.120	-5.472	12.95	-9.743
	$\bar{\alpha}\tilde{\chi}''_{eff}(\tilde{\gamma}_c,\bar{\alpha})$	0.434	10.701	-57.08	145.0	-127.9

TABLE IV: Parameters of $\tilde{\gamma}_c$, $\bar{\alpha}\tilde{\chi}_{eff}(\tilde{\gamma}_c,\bar{\alpha})$ and $\bar{\alpha}\tilde{\chi}''_{eff}(\tilde{\gamma}_c,\bar{\alpha})$ used in the fits and the predictions.

APPENDIX II: Renormalisation-scale variation effects on the triple differential cross section

In this Appendix, we show the renormalisation-scale variation effects on the triple differential cross section in the case of the NLL-BFKL S3 and CCS schemes. The results for the S4 schemes were displayed in Section IV and the conclusion that were obtained also holds for the S3 and CCS schemes. The corresponding comparisons with the data are shown in Fig.11 and Fig.12.

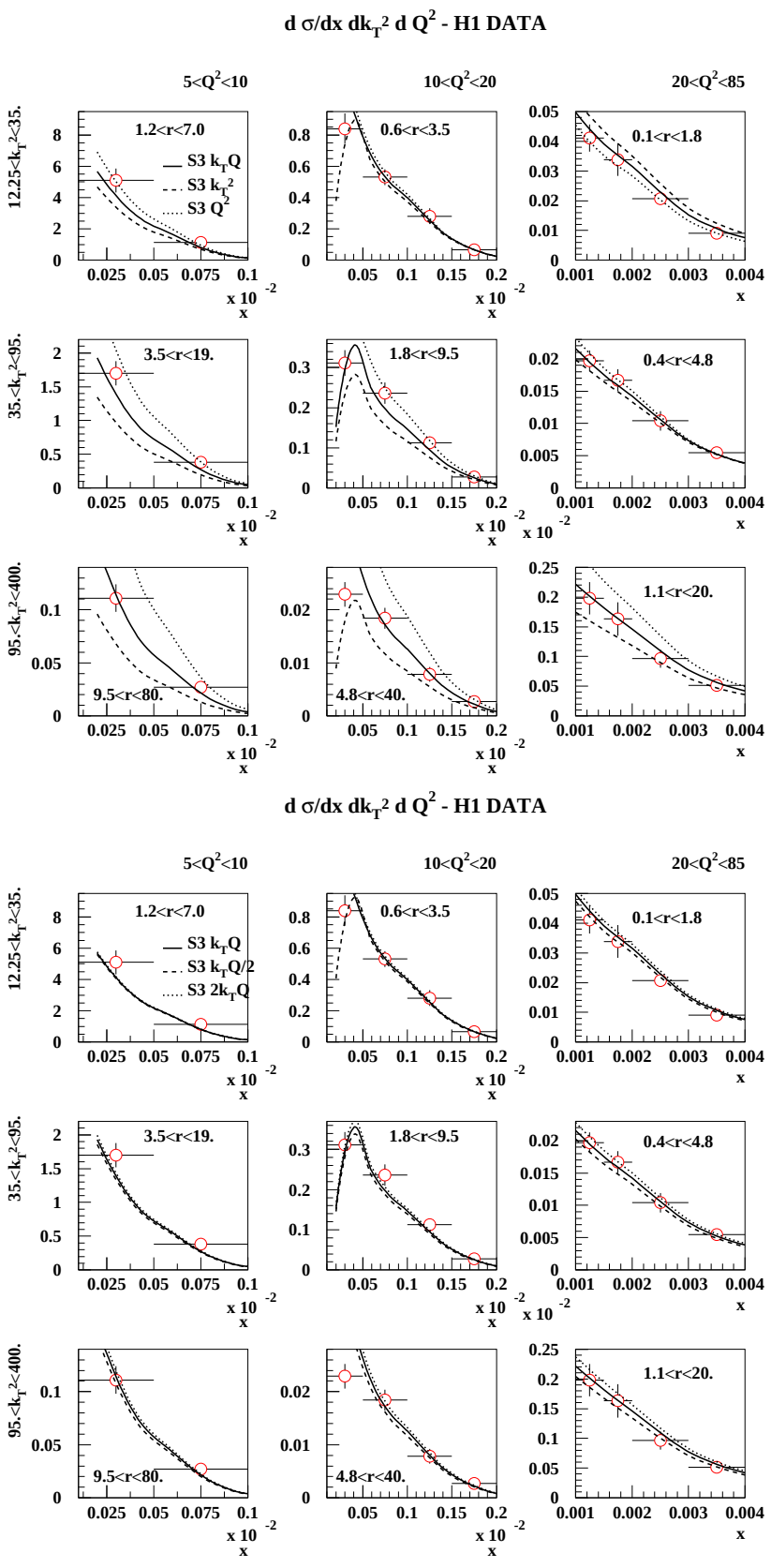

FIG. 11: Renormalisation-scale variation effects on the triple differential cross section for the S3 scheme. The relative normalisations coming from the $d\sigma/dx$ fits has been applied. Upper plot: $\lambda = (k_T/Q)^{\pm 1}$. Lower plot: $\lambda = 2^{\pm 1}$.

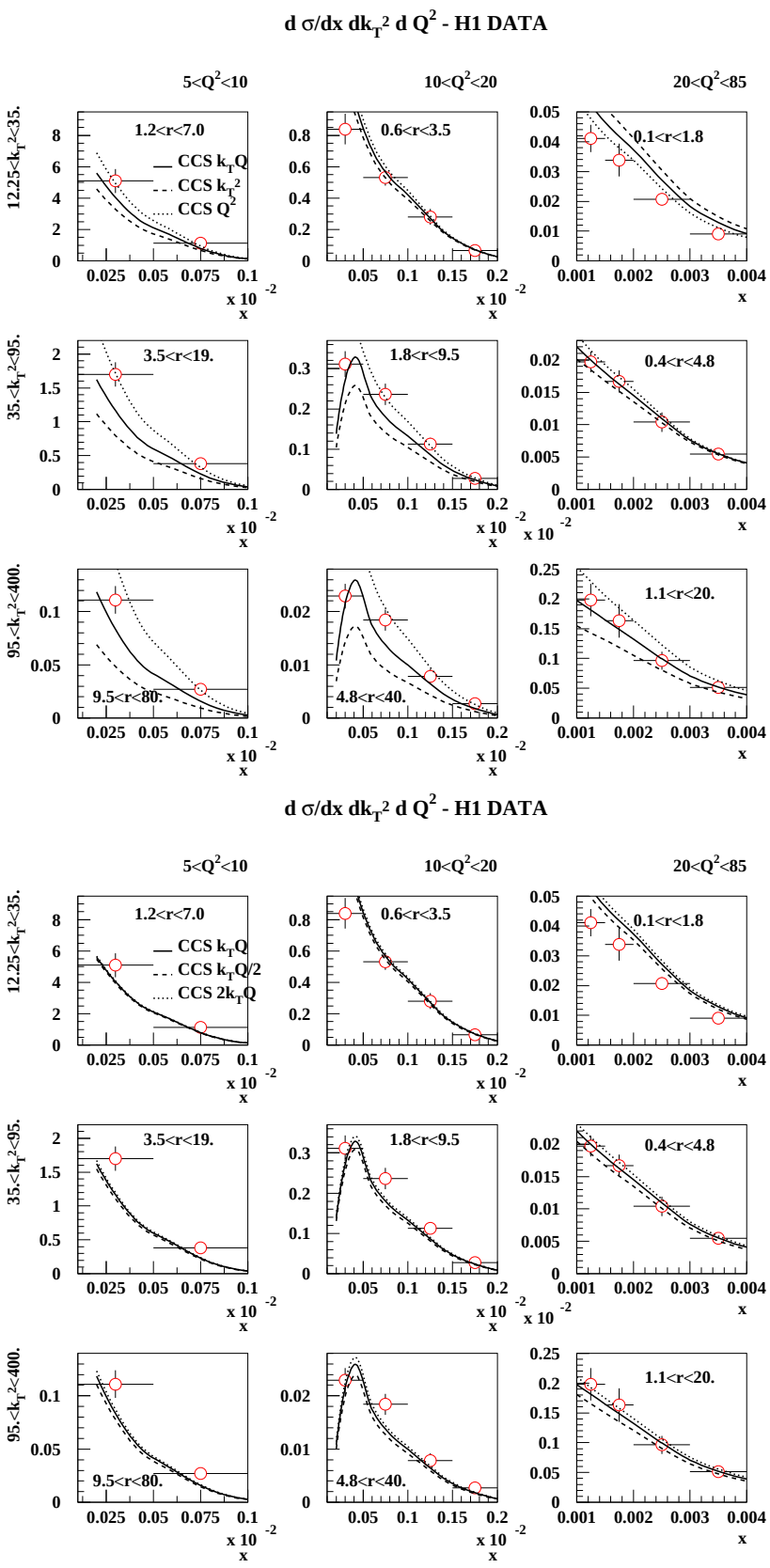

FIG. 12: Renormalisation-scale variation effects on the triple differential cross section for the CCS scheme. The relative normalisations coming from the $d\sigma/dx$ fits has been applied. Upper plot: $\lambda = (k_T/Q)^{\pm 1}$. Lower plot: $\lambda = 2^{\pm 1}$.

[1] A.H. Mueller, *J. Phys.* **G17** (1991) 1443.
[2] L.N. Lipatov, *Sov. J. Nucl. Phys.* **23** (1976) 338; E.A. Kuraev, L.N. Lipatov and V.S. Fadin, *Sov. Phys. JETP* **45** (1977) 199; I.I. Balitsky and L.N. Lipatov, *Sov. J. Nucl. Phys.* **28** (1978) 822.
[3] G. Altarelli and G. Parisi, *Nucl. Phys.* **B126** 18C (1977) 298; V.N. Gribov and L.N. Lipatov, *Sov. J. Nucl. Phys.* (1972) 438 and 675; Yu.L. Dokshitzer, *Sov. Phys. JETP* **46** (1977) 641.
[4] V.S. Fadin and L.N. Lipatov, *Phys. Lett.* **B429** (1998) 127; M. Ciafaloni, *Phys. Lett.* **B429** (1998) 363; M. Ciafaloni and G. Camici, *Phys. Lett.* **B430** (1998) 349.
[5] A. Aktas *et al* [H1 Collaboration], *Eur. Phys. J.* **C46** (2006) 27.
[6] S. Chekanov *et al* [ZEUS Collaboration], *Phys. Lett.* **B632** (2006) 13.
[7] C. Adloff *et al* [H1 Collaboration], *Nucl. Phys.* **B538** (1999) 3; J. Breitweg *et al* [ZEUS Collaboration], *Eur. Phys. J* **C6** (1999) 239.
[8] J.G. Contreras, R. Peschanski and C. Royon, *Phys. Rev.* **D62** (2000) 034006.
[9] H. Jung, L. Jonsson and H. Kuster, Eur. Phys. J. **C9** (1999) 383.
[10] C. Marquet and C. Royon, *Nucl. Phys.* **B739** (2006) 131.
[11] G.P. Salam, *JHEP* **9807** (1998) 019.
[12] M. Ciafaloni, D. Colferai and G.P. Salam, *Phys. Rev.* **D60** (1999) 114036; *JHEP* **9910** (1999) 017.
[13] S.J. Brodsky, V.S. Fadin, V.T. Kim, L.N. Lipatov and G.B. Pivovarov, *JETP Lett.* **70** (1999) 155; R.S. Thorne, *Phys. Rev.* **D60** (1999) 054031; G. Altarelli, R.D. Ball and S. Forte, *Nucl. Phys.* **B621** (2002) 359.
[14] J. Bartels, D. Colferai, S. Gieseke and A. Kyrieleis, *Phys. Rev.* **D66** (2002) 094017; V.S. Fadin, D.Yu. Ivanov and M.I. Kotsky, *Nucl. Phys.* **B658** (2003) 156; J. Bartels and A. Kyrieleis, *Phys. Rev.* **D70** (2004) 114003.
[15] R. Peschanski, C. Royon and L. Schoeffel, *Nucl. Phys.* **B716** (2005) 401.
[16] O. Kepka, C. Marquet, R. Peschanski and C. Royon, *Next-leading BFKL effects in forward-jet production at HERA*, hep-ph/0609299.
[17] Y.V. Kovchegov and A.H. Mueller, *Phys. Lett.* **B439** (1998) 428.
[18] M. Ciafaloni, D. Colferai, G.P. Salam and A.M. Stasto, *Phys. Rev.* **D68** (2003) 114003.
[19] Z. Nagy and Z. Trocsanyi, *Phys. Rev. Lett.* **87** (2001) 082001.
[20] J. Pumplin, D.R. Stump, J. Huston, H.L. Lai, P. Nadolsky and W.K. Tung, *JHEP* **0207** (2002) 012.
[21] A.H. Mueller and H. Navelet, *Nucl. Phys.* **B282** (1987) 727.
[22] C. Marquet and R. Peschanski, *Phys. Lett.* **B587** (2004) 201; C. Marquet, R. Peschanski and C. Royon, *Phys. Lett.* **B599** (2004) 236.